Variable Energy Photoelectron Spectroscopy of $M(\eta^3\text{-}C_3H_5)_2$ (M = Ni, Pd, and Pt): Molecular Orbital Assignments

Xiaorong Li, G. M. Bancroft,* R. J. Puddephatt,* Z. F. Liu, Y. F. Hu, and K. H. Tan

Contribution from the Department of Chemistry, University of Western Ontario, London, Canada N6A 5B7, and Canadian Synchrotron Radiation Facility, Synchrotron Radiation Center, University of Wisconsin—Madison, Stoughton, Wisconsin 53589

Received February 15, 1994. Revised Manuscript Received August 2, 1994®

Abstract: Variable energy valence and inner valence photoelectron spectra have been recorded between 21 and 170 eV using He I, He II, and synchrotron radiation for the bis(η^3-allyl) metal complexes $M(\eta^3\text{-}C_3H_5)_2$ (M = Ni, Pd, and Pt). MS–Xα–SW ground state and transition state calculations have been performed on the *trans* and *cis* structures. Photoionization cross sections have also been calculated for the valence ionizations of the three *trans* isomers, using both the Gelius and MS–Xα–SW methods. The theoretical branching ratios ($\sigma_i/\sum\sigma$) from both theoretical methods have been compared with the observed branching ratios between 21 and 170 eV. The orbital energies and orbitals characters for the *cis* complexes compared with the *trans* complexes indicate that our spectra are predominantly due to the *trans* complexes. For *trans*-$Ni(\eta^3\text{-}C_3H_5)_2$, our assignment (from the high-resolution He I and He II spectra and the good agreement between theoretical and observed branching ratios between 21 and 90 eV) gives the following orbital ordering: $13a_g$, $12a_g < 6b_g$, $7a_u < 11a_g < 5b_g < 11b_u < 10a_g$. This ordering is very different from that proposed from all previous experimental and theoretical assignments. In particular, the low binding energy peak at 7.64 eV is assigned to two orbitals, $13a_g$ and $12a_g$, of mainly Ni 3d character rather than the ligand $7a_u$ orbital. The $7a_u$ orbital contributes mainly to the second band at 8.1 eV. Apart from this discrepancy, our assignment of the MO ordering agrees with our Xα–SW energies. In contrast, the low binding energy peaks in the Pd and Pt analogues at 7.64 and 7.91 eV, respectively, arise from the ligand $8a_u$ and $12a_u$ orbitals as proposed earlier. The mainly 4d and 5d orbitals give rise to the next five peaks, with the two other b_g and a_g ligand orbitals giving the two high binding energy peaks (as for the Ni complex). For the Pd complex, the Pd 4d Cooper minimum in the cross sections at ~120 eV gives rise to spectacular variations in the branching ratios which make the assignment of ligand and metal orbitals rather easy. The major differences between the Ni, Pd, and Pt assignments are primarily due to the lower binding energy of the 3d electrons (Ni) compared to the 4d (Pd) and 5d (Pt) electrons. Reorganization effects apparently are not the dominant cause of the trend. The complete inner valence spectra of all three complexes have also been assigned to ligand orbitals with the aid of the Xα–SW energy calculations. Very unusual large intensity variations with the photon energy of the peak at 17.9 eV are probably due to dynamic correlation satellites.

Introduction

For many fundamentally important organometallic molecules such as $M(CO)_6$ (M = Cr, Mo, and W)[1] and $M(\eta^5\text{-}C_5H_5)_2$ (M = Fe, Ru, and Os),[2] the molecular orbital (MO) ordering assigned from photoelectron spectra and MO calculations is on a sound footing. However, for other important organometallic molecules, such as $M(\eta^3\text{-}C_3H_5)_2$ (M = Ni, Pd, and Pt), the MO ordering has been very controversial.[3] For example, for $Ni(\eta^3\text{-}C_3H_5)_2$, there have been many different assignments from experimental and theoretical studies in the last 24 years.[3] The controversy has centered firstly on the assignment of the low ionization energy peak at 7.8 eV and secondly on the validity of Koopmans' theorem for relating the measured IP's with the ground state MO energies. Despite experimental inconsistencies, all the latest experimental and theoretical studies[3d-t] have agreed that the peak at 7.8 eV arises from the ligand nonbonding $7a_u$ orbital rather than one (or more) of the Ni 3d orbitals. In contrast, Veillard initially assigned the first IP to a Ni 3d orbital[3a] but later[3e] showed from ab initio calculations that the Ni 3d relaxation energies can be *much larger* than those for the ligand orbitals. Thus, while the Ni 3d orbital might still be assigned to the first peak(s),[3e] the ligand $7a_u$ orbital was certainly still considered to be the HOMO in the ground state.

These large "differential" relaxation effects and correlation effects (reorganization energies) are now generally recognized in the literature,[3-5] although Xα–SW calculations on $Ni(\eta^3\text{-}C_3H_5)_2$[3k,t] have shown that the ground state and transition state orderings of MO's are the same, suggesting strongly that such differential reorganization energies are not nearly as large, or important, as is usually claimed.

* To whom correspondence should be addressed at the University of Western Ontario.

® Abstract published in *Advance ACS Abstracts*, September 15, 1994.

(1) Cooper, G.; Green, J. C.; Payne, M. P.; Dobson, B. R.; Hillier, I. H. *J. Am. Chem. Soc.* **1987**, *109*, 3836.

(2) Cooper, G.; Green, J. C.; Payne, M. P. *Mol. Phys.* **1988**, *63*, 1031.

(3) (a) Veillard, A. *J. Chem. Soc. D* **1969**, 1022. (b) Lloyd, D. R.; Lynaugh, N. *Proc. Int. Conf. Electron Spectrosc.* **1971**, 445. (c) Batich, C. D. *J. Am. Chem. Soc.* **1976**, *98*, 7585. (d) Brown, D. A.; Owens, A. *Inorg. Chim. Acta* **1971**, *5*, 675. (e) Rohmer, M.-M.; Veillard, A. *J. Chem. Soc., Chem. Commun.* **1973**, 250. (f) Rohmer, M.-M.; Demuynck, J.; Veillard, A. *Theor. Chim. Acta* **1974**, *36*, 93. (g) Böhm, M. C.; Gleiter, R.; Batich, C. D. *Helv. Chim. Acta* **1980**, *63*, 990. (h) Böhm, M. C.; Gleiter, R. *Theor. Chim. Acta* **1980**, *57*, 315. (i) Green, J. C. *Struct. Bonding* **1981**, *43*, 37. (j) Böhm, M. C.; Gleiter, R. *Chem. Phys.* **1982**, *64*, 183. (k) Hancock, G. C.; Kostić, N. M.; Fenske, R. F. *Organometallics* **1983**, *2*, 1089. (l) Goddard, R.; Krüger, C.; Mark, F.; Stansfield, R.; Zhang, X. *Organometallics* **1985**, *4*, 285. (m) Moncrieff, D.; Hillier, I. H.; Saunders, V. R.; von Niessen, W. *J. Chem. Soc., Chem. Commun.* **1985**, 779. (n) Moncrieff, D.; Hillier, I. H.; Saunders, V. R.; von Niessen, W. *Inorg. Chem.* **1985**, *24*, 4247. (o) Böhm, M. C.; Gleiter, R. *Chem. Phys. Lett.* **1986**, *123*, 87. (p) Moncrieff, D.; Hillier, I. H.; Saunders, V. R.; von Niessen, W. *Chem. Phys. Lett.* **1986**, *131*, 545. (q) Hillier, I. H. *Quantum Chemistry: The Challenge of Transition Metals and Coordination Chemistry*; NATO ASI Series C; D. Reidel Publishing Co.: Hingham, 1986; pp 143. (r) Decleva, P.; Fronzoni, G.; Dealti, G.; Lisini, A. *J. Mol. Struct.* **1989**, *184*, 49. (s) Decleva, P.; Fronzoni, G.; Lisini, A. *Chem. Phys.* **1989**, *134*, 307. (t) Guerra, M; Jones, D.; Distefano, G.; Torroni, S.; Foffani, A.; Modelli, A. *Organometallics* **1993**, *12*, 2203.

(4) Lichtenberger, D. L.; Calabro, D. C; Kellogg, G. E. *Organometallics* **1984**, *3*, 1623.

(5) (a) Calabro, D. C.; Lichtenberger, D. L. *Inorg. Chem.* **1980**, *19*, 1732. (b) Lichtenberger, D. L.; Kellogg, G. E. *Acc. Chem. Res.* **1987**, *20*, 379.

0002-7863/94/1516-9543$04.50/0

Despite the very large qualitative differences in the He I and He II spectra of $Ni(\eta^3\text{-}C_3H_5)_2$ compared to the Pd and Pt analogues, the assignment of the Pd and Pt spectra has been much less controversial.[3g,t] However, to our knowledge, there have been only two calculations on $Pd(\eta^3\text{-}C_3H_5)_2$ (one over 20 years ago[6] and one very recently[3t]) and there have been no calculations on $Pt(\eta^3\text{-}C_3H_5)_2$.

With the advent of synchrotron radiation sources, it has become possible in the last 10 years to obtain high-quality valence band photoelectron spectra at continuously variable photon energy for small inorganic molecules[7] and transition metal complexes.[1,2,8] Because photoionization cross sections for different atomic and molecular orbital vary greatly with photon energy (due, for example, to delayed onsets, shape resonances, Cooper minima, and many body effects[9]), the relative intensities of photoelectron peaks usually vary markedly with photon energy. Comparison of the experimental *intensities* (or relative intensities) with theoretical values usually enables a much more confident assignment of the photoelectron peaks[7,8] than is possible just using experimental and theoretical *energies*.

In this paper, we have carried out a detailed variable energy gas phase photoelectron study of the three compounds $M(\eta^3\text{-}C_3H_5)_2$ (M = Ni, Pd, and Pt) using He I, He II, and monochromatized synchrotron radiation sources. We have also performed MS–Xα ground state and transition state calculations on all three compounds and have compared the experimental intensity variations with theoretical intensities from the Gelius model and MS–Xα intensity calculations. We had three objectives. First, we wanted to confirm the valence band assignment of the photoelectron spectra for all three compounds. Second, we wanted to investigate the reorganization energy contributions to the spectral IP's for all three compounds and hopefully obtain a more confident assignment of the orbital energies in the ground state. Third, we wanted to study the inner valence photoelectron spectra for the first time and assign all of the peaks. Preliminary accounts of parts of this work have been communicated.[10]

Experimental Section

The compounds were synthesized by methods in the literature.[11-13] Samples were purified by vacuum sublimation before recording the NMR and PES spectra and were stored at −78 °C under an inert atmosphere. $Ni(\eta^3\text{-}C_3H_5)_2$ is easily decomposed by oxygen but is easily sublimed without decomposition in the absence of oxygen. The ^1H NMR spectrum of $Ni(\eta^3\text{-}C_3H_5)_2$ confirms the purity of $Ni(\eta^3\text{-}C_3H_5)_2$ used in our work.[11-13]

All samples were introduced into the gas cell of two different photoelectron spectrometers by sublimation. For the Ni, Pd, and Pt compounds, the sublimation temperatures used were −28 (from a NaBr/ice bath), 10, and 22 °C, respectively. The He I and He II spectra of the compounds were obtained using an ESCA 36 spectrometer with a resolution of ~20 meV.[14] The variable energy spectra from 20 to 170 eV were obtained at the Canadian Synchrotron Radiation Facility (CSRF) at the Aladdin storage ring using a modified ESCA 36 spectrometer fitted with a Quantar #36 position sensitive detector.[15,16] The Grasshopper grazing incidence monochromator has been previously described.[17] Briefly, photoelectrons were collected at the pseudomagic angle calculated assuming 90% polarization of the synchrotron light. This ensures that the photoelectron intensities obtained are independent of well-known angular effects. Differential pumping of the gas cell maintains a pressure differential of better than 10^4 between the gas cell and the energy analyzer. A light pipe separating the gas cell from the grasshopper monochromator further ensures long-term stability of the system. Many broad scan and narrow scan spectra of both valence and inner valence regions were recorded between 20 and 170 eV of photon energy at a resolution of *ca.* 100 meV between 20 and 80 eV and *ca.* 500 meV between 80 and 170 eV. The He I spectrum was calibrated with the Ar $3p_{3/2}$ line at 15.759 eV. For the synchrotron radiation spectra, the Xe 5s mainline at 23.397 eV was used as the calibrant.

For the cross section analyses, many of the spectra were fit to Gaussian–Lorentzian line shapes using an iterative procedure.[18] Peak positions, widths, and shapes were normally constrained to obtain consistent fits from one photon energy to another. Correction of the areas for the electron analyzer transmission was performed by dividing the computed area by the kinetic energy of the band. Experimental branching ratios (BR_i) were obtained using the resulting band areas, A_i, and the branching ratio formula, $BR_i = A_i/\sum A$.

Computational Details

Valence orbital energies and compositions of *trans*- and *cis*-$M(\eta^3\text{-}C_3H_5)_2$ (M = Ni, Pd, and Pt) were calculated using the Xα–SW method as described earlier.[19] Geometrical data for *trans*-$Ni(\eta^3\text{-}C_3H_5)_2$ were taken from the literature,[31] and structural parameters for *trans*-$Pd(\eta^3\text{-}C_3H_5)_2$ were taken from crystallographic data of *trans*-$Pd(\eta^3\text{-}CH_3C_3H_4)_2$.[20] The hydrogen atoms are bent away from the allyl planes.[31] Since no structural information is available for *trans*-$Pt(\eta^3\text{-}C_3H_5)_2$, by considering that the atomic radii for Pd (1.79 Å) and Pt (1.83 Å) are very similar,[21] we just used the same crystal parameters for the *trans*-Pt compound as for *trans*-$Pd(\eta^3\text{-}C_3H_5)_2$, except that the distance between the Pt atom and allyl plane is increased by 0.04 Å. C_{2h} and C_{2v} symmetry was assumed for all *trans* and *cis* isomers, respectively.

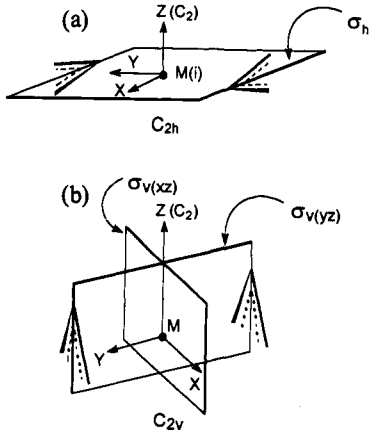

(6) Hillier, I. H.; Canadine, R. M. *Discuss. Faraday Soc.* **1969**, *47*, 27.
(7) For example: (a) Yates, B. W.; Tan, K. H.; Bancroft, G. M.; Coatsworth, L. L.; Tse, T. S. *J. Chem. Phys.* **1985**, *83*, 4906. (b) Yates, B. W.; Tan, K. H.; Bancroft, G. M.; Coatsworth, L. L.; Tse, T. S.; Schrobilgen, G. J. *J. Chem. Phys.* **1986**, *84*, 3603. (c) Addison-Jones, B. M.; Tan, K. H.; Yates, B. W.; Cutler, J. N.; Bancroft, G. M.; Tse, J. S. *J. Electron Spectrosc. Relat. Phenom.* **1989**, *48*, 155. (d) Bozek, J. D.; Cutler, J. N.; Bancroft, G. M.; Tan, K. H.; Yates, B. W.; Tse, J. S. *Chem. Phys.* **1989**, *132*, 257.
(8) (a) Didziulis, S. V.; Cohen, S. L.; Butcher, K. D.; Solomon, E. I. *Inorg. Chem.* **1988**, *27*, 2238. (b) Didziulis, S. V.; Cohen, S. L.; Gerwith, A. A.; Solomon, E. I. *J. Am. Chem. Soc.* **1988**, *110*, 250. (c) Butcher, K. D.; Didziulis, S. V.; Briat, B.; Solomon, E. I. *J. Am. Chem. Soc.* **1990**, *112*, 2231. (d) Brennan, J. G.; Green, J. C.; Redfarn, C. M. *J. Am. Chem. Soc.* **1989**, *111*, 2373. (e) Brennan, J. G.; Green, J. C.; Redfarn, C. M.; MacDonald, M. A. *J. Chem. Soc., Dalton Trans.* **1990**, 1907. (f) Lichtenberger, D. L.; Ray, C. D.; Stepniak, F.; Chen, Y.; Weaver, J. H. *J. Am. Chem. Soc.* **1992**, *114*, 10492.
(9) Berkowitz, J. *Photoabsorption, Photoionization, and Photoelectron Spectroscopy*; Academic Press: New York, 1979; pp 35–72.
(10) (a) Li, X.; Bancroft, G. M.; Puddephatt, R. J.; Hu, Y. F.; Liu, Z. F.; Tan, K. H. *Inorg. Chem.* **1992**, *31*, 5162. (b) Li, X.; Bancroft, G. M.; Puddephatt, R. J.; Hu, Y. F.; Liu, Z. F.; Sutherland, D. G. J.; Tan, K. H. *J. Chem. Soc., Chem. Commun.* **1993**, 67.
(11) Becconsall, J. K.; Job, B. E.; O'Brien, S. *J. Chem. Soc. A*, **1967**, 423.
(12) Bönnemann, H.; Bogdanović, B.; Wilke, G. *Angew. Chem.* **1967**, *79*, 817.
(13) Henc, B.; Jolly, P. W.; Salz, R.; Wilke, G.; Benn, R.; Hoffmann, E. G.; Mynott, R.; Schroth, G.; Seevogel, K.; Sekutowski, J. C.; Krüger, C. *J. Organomet. Chem.* **1980**, *191*, 425.
(14) Bancroft, G. M.; Bristow, D. J.; Coatsworth, L. L. *Chem. Phys. Lett.* **1981**, *82*, 344.
(15) Bozek, J. D.; Cutler, J. N.; Bancroft, G. M.; Coatsworth, L. L.; Tan, K. H.; Yang, D. S. *Chem. Phys. Lett.* **1990**, *165*, 1.
(16) Liu, Z. F.; Coatsworth, L. L.; Tan, K. H. *Chem. Phys. Lett.* **1993**, *203*, 337.
(17) Tan, K. H.; Bancroft, G. M.; Coatsworth, L. L.; Yates, B. W. *Can. J. Phys.* **1982**, *60*, 131. Bancroft, G. M.; Bozek, J. D.; Tan, K. H. *Phys. Can.* **1987**, 113.

For both *cis* and *trans* structures, the *z*-axis was assumed to be along the C_2 axis, and the *y*-axis perpendicular to the allyl planes, with the metal atom located at the origin. Since there is no crystal structure for a *cis* isomer, the structural parameters for all *cis* isomers were deduced by performing a reflection operation for one allyl radical in the *xz* plane of the *trans* isomer. The exchange α-parameters used in each atomic region were taken from Schwarz's tabulation,[22] except for hydrogen, for which 0.777 25 was used. Overlapping atomic sphere radii were used with the outsphere radius tangent to the outermost atomic spheres. An l_{max} of 4 was used around the outer sphere region, whereas l_{max} values of 3, 1, and 0 were used around M (Ni, Pd, and Pt), C, and H atoms, respectively. Photoionization cross sections were calculated for the outer valence levels of *trans*-M(η^3-C_3H_5)$_2$, using the Xα–SW cross section program of Davenport.[23] The calculations were performed with the converged Xα–SW HOMO transition state potential and modified with a Latter tail to correct for large r behavior. In addition to the parameters used in the Xα–SW calculations on molecular orbitals, the maximum azimuthal quantum numbers, l_{max}, for final states were extended to 8, 4, 2, and 1 around outersphere, metal, carbon, and hydrogen regions, respectively. In calculations of transition states, one-half of an electron is removed from each of the eight uppermost molecular orbitals and no Watson sphere was used in the calculation on the transition states. All symmetry-allowed photoionization processes based on the dipolar selection rule were included in the calculations.

Results

(a) The Photoelectron Spectra. The He I photoelectron spectra of the three compounds are shown in Figure 1. These spectra are essentially identical (see Table 1 for the IP's) to those already presented in the literature by many workers.[3] The first three bands in Ni(η^3-C_3H_5)$_2$ and the first two bands in Pd(η^3-C_3H_5)$_2$ are broad and asymmetric, so we recorded very narrow scan He I and He II spectra of these complexes to further resolve features in these spectra (Figures 2 and 3). Several new features which have not been noted in the literature are evident. For example, an additional peak 2A is clearly evident in this first He II spectrum of Ni(η^3-C_3H_5)$_2$ and five peaks (corresponding to the five MO's) can readily be fit consistently to both He I and He II spectra. Peak 6 is very broad for Pd(η^3-C_3H_5)$_2$ and must be composed of two bands. Thus all three compounds yield the eight peaks expected from the eight MO's (Table 1 and the next section).

A detailed examination of the first two He I peak profiles of Pd(η^3-C_3H_5)$_2$ is also informative. A two-peak fit is inadequate: the peaks are both asymmetric. The fit in Figure 3 gives the best fit with the least number of peaks. These fits are certainly those expected from a vibrational progression, and the vibrational frequencies derived from these fits vary from 1150 to 1300 cm^{-1}, close to the ground state vibrational frequencies 1009–1029 cm^{-1} of the C–C–C vibrational modes for solid state Pd(η^3-C_3H_5)$_2$.[24]

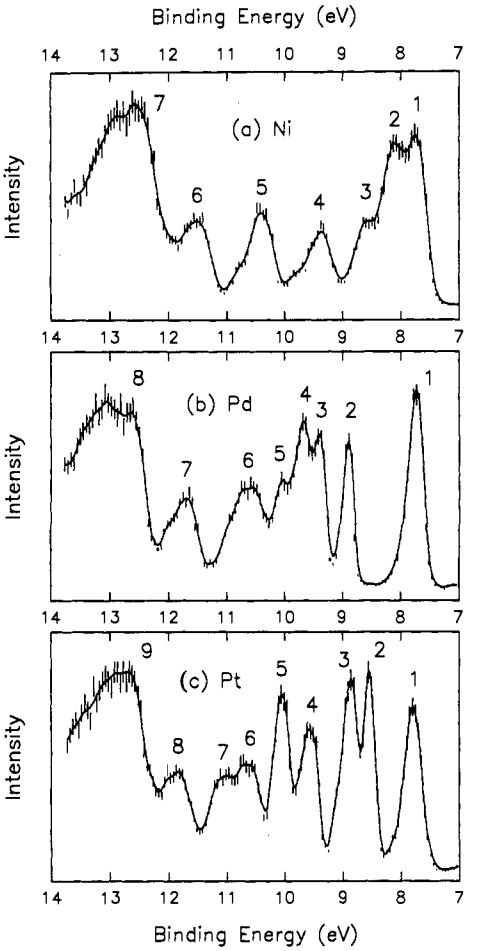

Figure 1. He I valence band photoelectron spectra of the three M(η^3-C_3H_5)$_2$ (M = Ni, Pd, and Pt) complexes. The solid line links the smoothed data.

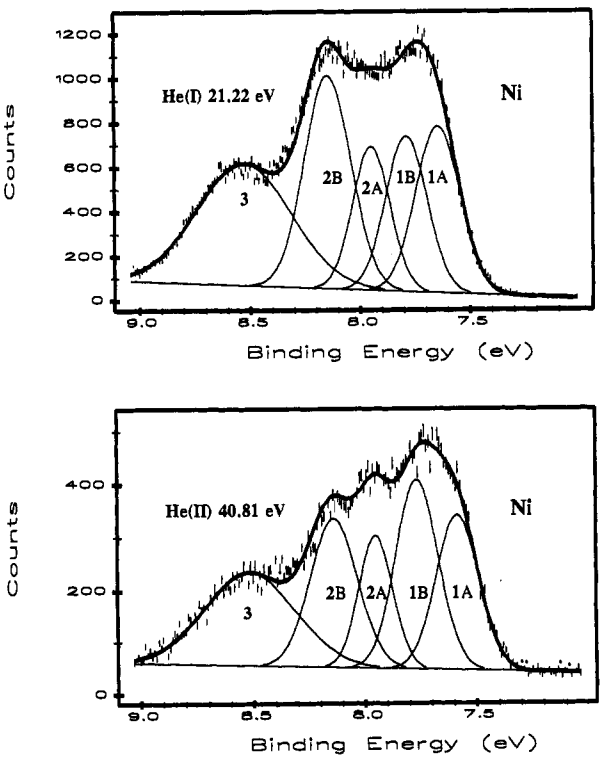

Figure 2. High-resolution He I and He II spectra of Ni(η^3-C_3H_5)$_2$ showing the first three valence bands in more detail.

Representative variable energy spectra for the three compounds are shown in Figures 4–8. The higher resolution spectra (Figures

(18) Bancroft, G. M.; Adams, J.; Coatsworth, L. L.; Bennewitx, C. D.; Brown, J. D.; Westwood, W. D. *Anal. Chem.* **1975**, *47*, 586.

(19) (a) Yang, D. S.; Bancroft, G. M.; Puddephatt, R. J.; Bozek, J. D.; Tse, J. S. *Inorg. Chem.* **1989**, *28*, 1. (b) Yang, D. S.; Bancroft, G. M.; Puddephatt, R. J.; Bursten, B. E.; McKee, S. D. *Inorg. Chem.* **1989**, *28*, 872. (c) Yang, D. S.; Bancroft, G. M.; Puddephatt, R. J. *Inorg. Chem.* **1990**, *29*, 2118. (d) Yang, D. S.; Bancroft, G. M.; Dignard-Bailey, L.; Puddephatt, R. J.; Tse, J. S. *Inorg. Chem.* **1990**, *29*, 2487. (e) Yang, D. S.; Bancroft, G. M.; Puddephatt, R. J.; Tse, J. S. *Inorg. Chem.* **1990**, *29*, 2496. Yang, D. S.; Bancroft, G. M.; Puddephatt, R. J.; Tan, K. H.; Cutler, J. N.; Bozek, J. B. *Inorg. Chem.* **1990**, *29*, 4956.

(20) Gozum, J. E.; Pollina, D. M.; Jensen, J. A.; Girolami, G. S. *J. Am. Chem. Soc.* **1988**, *110*, 2688.

(21) *Table of Periodic Properties of the Elements*; Sargent-Welch Scientific Co.: Skokie, IL, 1980.

(22) (a) Schwarz, K. *Phys. Rew. B* **1972**, *5*, 2466. (b) Schwarz, K. *Theor. Chim. Acta* **1974**, *34*, 225.

(23) (a) Davenport, J. W. Ph.D. Dissertation, University of Pennsylvania, Philadelphia, PA, 1976. (b) Davenport, J. W. *Phys. Rev. Lett.* **1976**, *36*, 945.

(24) Andrews, D. C.; Davidson, G. J. *J. Organomet. Chem.* **1973**, *55*, 383.

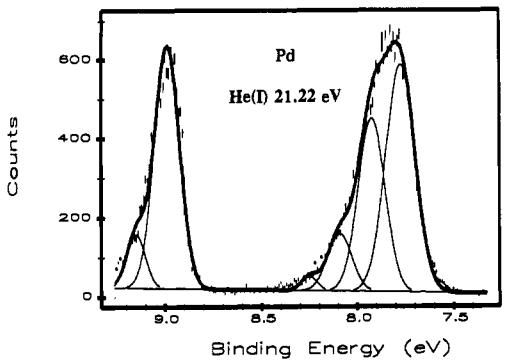

Figure 3. High-resolution He I spectrum of $Pd(\eta^3\text{-}C_3H_5)_2$ showing the first two bands in more detail.

Table 1. Xα–SW MO Compositions (for the *trans* Isomer) and PES Band Assignment of $M(\eta^3\text{-}C_3H_5)_2$

Ni orbital	Xα energy (eV)	IP (eV, ±0.02)	band assignment	Ni %4s	Ni %4p	Ni %3d	middle C %p	terminal C %p
$7a_u$	−4.39	8.15	2B		13.4			83.1
$13a_g$	−5.00	7.64	1A	3.9		90.9		
$12a_g$	−5.09	7.79	1B			94.9		
$6b_g$	−5.21	7.95	2A			98.0		
$11a_g$	−5.60	8.52	3			93.0		
$5b_g$	−6.24	9.38	4			69.1	3.4	26.2
$11b_u$	−6.64	10.36	5		8.20		45.0	41.3
$10a_g$	−7.98	11.48	6	13.7		4.2	32.4	38.8
Pd orbital	**Xα energy (eV)**	**IP (eV, ±0.02)**	**band assignment**	**Pd %5s**	**Pd %5p**	**Pd %4d**	**middle C %p**	**terminal C %p**
$8a_u$	−3.29	7.64	1		10.5			85.4
$17a_g$	−5.62	8.81	2	12.5		68.8	4.1	13.0
$13b_u$	−5.76	10.58	6		6.5		47.8	42.3
$16a_g$	−6.44	9.28	3			93.4		
$8b_g$	−6.65	9.58	4			96.7		
$15a_g$	−6.88	9.96	5			92.4	4.5	1.3
$7b_g$	−7.18	10.58	6			72.2	6.3	19.6
$14a_g$	−7.39	11.65	7	3.5		40.2	23.5	26.0
Pt orbital	**Xα energy (eV)**	**IP (eV, ±0.02)**	**band assignment**	**Pt %6s**	**Pt %6p**	**Pt %5d**	**middle C %p**	**terminal C %p**
$12a_u$	−3.26	7.91	1		12.7			82.9
$21a_g$	−5.61	8.64	2	17.2		63.9	3.3	13.3
$19b_u$	−5.73	11.15	7		8.1		46.9	41.5
$20a_g$	−6.54	8.95	3			90.8	2.7	3.9
$10b_g$	−6.81	9.65	4			95.3		
$19a_g$	−7.08	10.14	5			86.9	7.5	2.5
$9b_g$	−7.38	10.73	6			65.9	8.5	22.8
$18a_g$	−7.50	11.90	8	3.3		44.2	20.2	24.7

4–6) show large intensity variations. In particular, the spectra show that the relative intensity of the first peak changes very differently for $Ni(\eta^3\text{-}C_3H_5)_2$ than for its Pd and Pt analogues: this peak increases in relative intensity from 21 to 70 eV for Ni, while for Pd and Pt, the intensity of peak 1 decreases dramatically. Of greater importance, the relative intensities vary smoothly over this whole energy range, as will be demonstrated later by the trends in branching ratios. This evidence shows immediately that the assignment of the first peak in $Ni(\eta^3\text{-}C_3H_5)_2$ *must* be different from those of the Pd and Pt analogues, contrary to *all* the recent literature.[3]

Finally, lower resolution spectra of the Ni and Pd compounds were obtained between 90 and 170 eV (Figures 7 and 8). The spectra of $Ni(\eta^3\text{-}C_3H_5)_2$ show that the relative intensities of bands 4, 5, and 6 continue to drop at higher energies. The behavior of the intensities for $Pd(\eta^3\text{-}C_3H_5)_2$ is quite different and perhaps surprising: band 1 drops greatly in relative intensity from 21 to 90 eV and then increases greatly to ~130 eV, before dropping again.

(b) Electronic Structures of *trans*-$M(\eta^3\text{-}C_3H_5)_2$ from Xα–SW Calculations: MO Ordering. The *trans* bis(π-allyl) fragment in

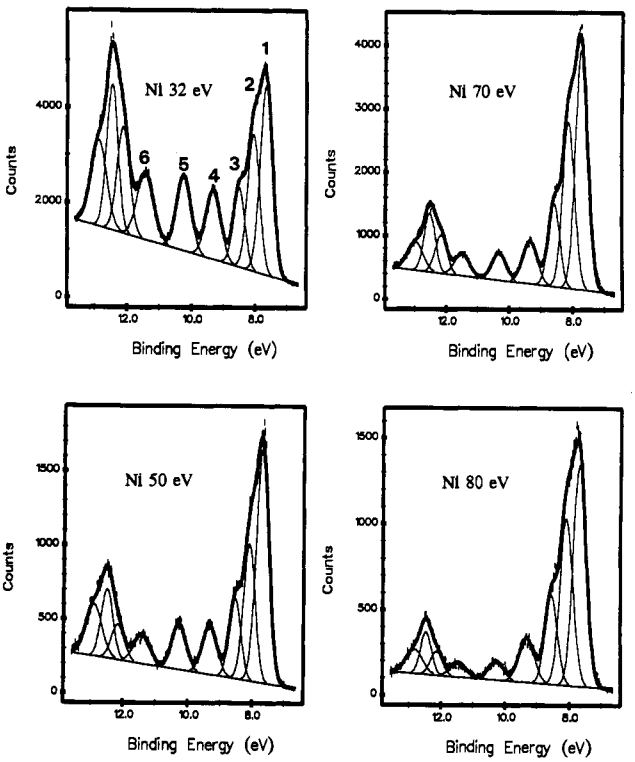

Figure 4. Representative valence band photoelectron spectra of $Ni(\eta^3\text{-}C_3H_5)_2$ at 32, 50, 70, and 80 eV.

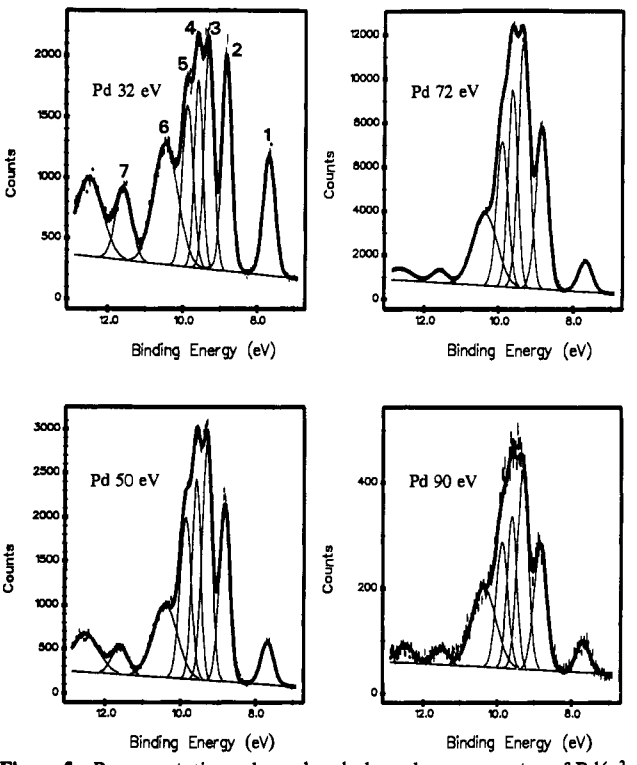

Figure 5. Representative valence band photoelectron spectra of $Pd(\eta^3\text{-}C_3H_5)_2$ at 32, 50, 72, and 90 eV.

$M(\eta^3\text{-}C_3H_5)_2$ has C_{2h} symmetry, and its four π molecular orbitals are in-phase and out-of-phase combinations of the molecular orbitals of the two individual allyl radical groups. Their electron configurations are $(core)(a_g)^2(b_u)^2(a_u)^2(b_g)^0$. These four ligand orbitals combine with the metal d orbitals to form the outer valence region of *trans*-$M(\eta^3\text{-}C_3H_5)_2$. Among the ligand π orbitals, two orbitals ($a_u(\pi)$ and $b_u(\pi)$) have odd parity (u) and hence cannot interact with the metal d and empty $(n+1)$s orbitals since they are all even (g). The symmetries of these two π orbitals match with a_u (p_z) and b_u (p_x and p_y) metal empty orbitals, respectively.

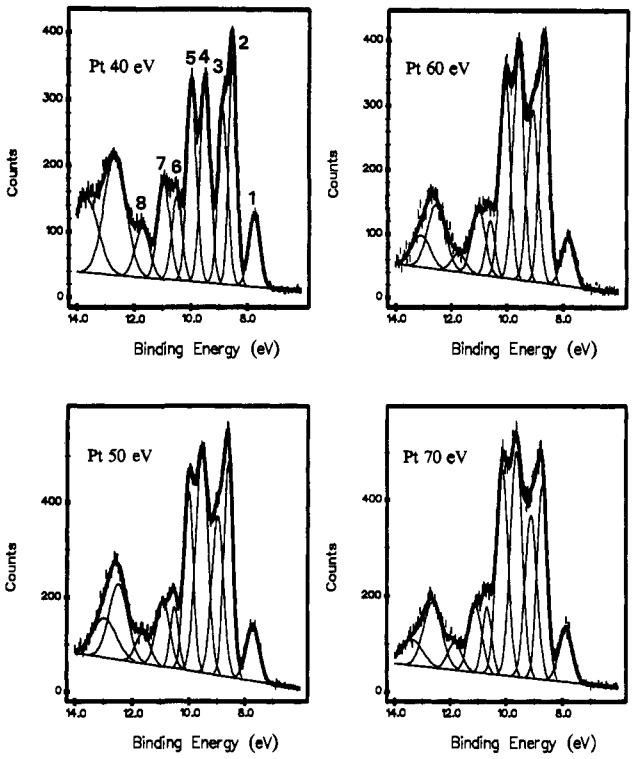

Figure 6. Representative valence band photoelectron spectra of $Pt(\eta^3\text{-}C_3H_5)_2$ at 40, 50, 60, and 70 eV.

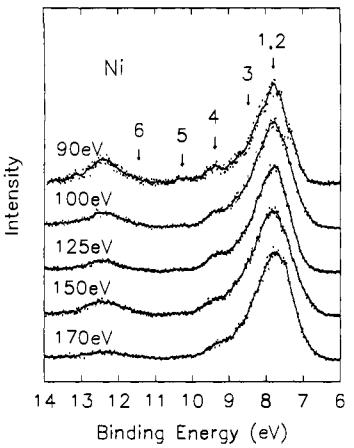

Figure 7. Valence band photoelectron spectra of $Ni(\eta^3\text{-}C_3H_5)_2$ from 90 to 170 eV. All spectra are normalized to the height of bands 1 and 2.

And a_g (π) and b_g (π) have the proper symmetry to mix with a_g (d_{xy}, d_{z^2}, and $d_{x^2-y^2}$) and b_g (d_{xz} and d_{yz}) metal orbitals, respectively. The qualitative analysis of symmetry, energy, and overlap requirements for bonding has shown that most MO's in *trans*-$Ni(\eta^3\text{-}C_3H_5)_2$ are essentially nonbonding. Only the ligand empty b_g (π) has a tendency to bond with one of Ni 3d orbital in b_g symmetry.[3c,g]

The results from the present ground state and transition state calculations on the three molecules are given in Tables 1 and 2 and Figure 9. Our results give an orbital sequence very similar to those in the two previous Xα calculations,[3k,t] although Fenske's calculations were performed with the H atoms in the allyl plane. Our calculations on both "bent" and "flat" geometries are very similar, but the trend for the "flat" calculation is in even better agreement with Fenske's.[3k]

Indeed, our transition state energies (which should approximate the IP's[3k]) and sequences (Table 2) for Ni and Pd molecules are in good agreement with those published independently very recently.[3t] The orbital *sequences* for the ground state energies found here are very similar to those found in Fenske's earlier Xα calculations, although the absolute energies differ. However,

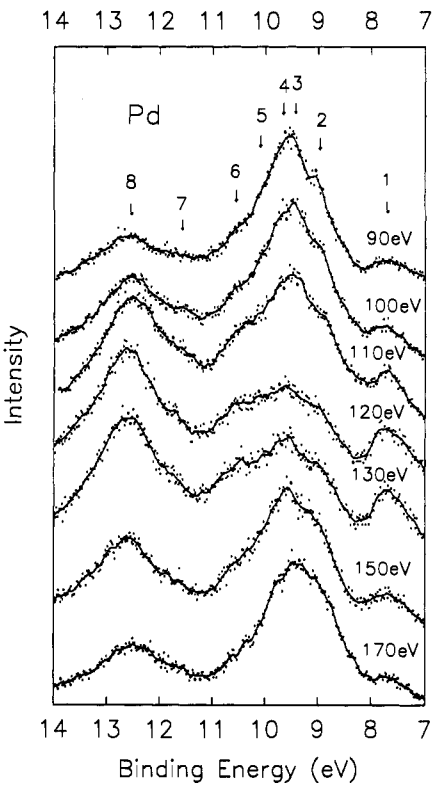

Figure 8. Valence band photoelectron spectra of $Pd(\eta^3\text{-}C_3H_5)_2$ from 90 to 170 eV.

the orbital sequences in ground *and* transition states are quite different from those of other calculational methods.[3] More importantly, the order of energies does not change significantly from the ground to transition state (Table 2).

The orbital characters for the different MO's in Table 1 are also very similar to those found in the two previous Xα calculations. Only the $5b_g$ MO (26.2% C 2p and 69.1% Ni 3d), which is formed by overlap of the empty $b_g(\pi)$ orbital of the bis(π-allyl) fragment with a Ni 3d orbital of b_g symmetry, possesses significant bonding character. All other outer valence MO's retain the character of either ligand π (more than 70% C 2p) or Ni 3d (more than 90% Ni 3d) character. In contrast, the ab initio[3f] and INDO[3h] methods give substantially more mixing of the Ni 3d and ligand orbitals.

Note that the ligand a_u orbital is at high energy for *all three* molecules in *both* ground and transition states. For the nickel complex, the five orbitals of mostly 3d character are calculated to lie in the region −5.0 to −6.2 eV, where they lie between the ligand a_u (HOMO) and b_u orbital levels. However, for M = Pd or Pt, the d orbitals are at lower energy (−5.62 to −7.18 eV for Pd, −5.61 to −7.38 eV for Pt) and all but one lie below the ligand b_u level as shown in Figure 9. Because of the better energy match, there is stronger mixing between the metal d and ligand π orbitals of a_g symmetry for M = Pd or Pt than for M = Ni (see orbitals $14a_g$ for Pd and $18a_g$ for Pt in Table 1).

(c) Theoretical Trends in Photoelectron Cross Sections. We obtained theoretical cross sections using both the Gelius method[25] and the Xα method using Davenport's program[23] and then obtained branching ratios ($BR_i = \sigma_i/\sum\sigma$) where σ_i is the calculated cross section to compare with the experimental BR_i values. In the Gelius treatment, the cross section of an individual MO is assumed to be proportional to the sum of the atomic cross sections (σ_{A_j}) of its components weighted by the "probability" $(P_{A_j})_i$ of finding the ith molecular orbital an electron belonging to the atomic orbital A_j:

(25) (a) Gelius, U. *Electron Spectroscopy*; Shirley, D. A., Ed.; North Holland: Amsterdam, 1972; pp 311. (b) Bancroft, G. M.; Malmquist, P.-A.; Svensson, S.; Basilier, E.; Gelius, U.; Siegbahn, K. *Inorg. Chem.* **1978**, *17*, 1595.

Table 2. Differences (Δ) between Transition State Eigenvalues (E_T) and Ground State Eigenvalues (E_G) in *trans*-Ni(η^3-C_3H_5)$_2$ and *trans*-Pd(η^3-C_3H_5)$_2$[a]

trans-Ni(η^3-C_3H_5)$_2$									*trans*-Pd(η^3-C_3H_5)$_2$					
orbital	%Ni 3d	E_T	E_G	Δ	E_T'	E_G'	Δ'	E_T''	orbital	%Pd 4d	E_T	E_G	Δ	E_T''
$7a_u$		-6.84	-4.39	-2.45	-2.48	-0.14	-2.34	-7.0	$8a_u$		-5.71	-3.29	-2.42	-6.9
$13a_g$	90.9	-8.43	-5.00	-3.43	-4.50	-1.31	-3.19	-8.2	$17a_g$	68.8	-8.39	-5.62	-2.77	-8.9
$12a_g$	94.9	-8.77	-5.09	-3.68	-5.21	-1.76	-3.45	-8.8	$13b_u$		-8.35	-5.76	-2.59	-10.3
$6b_g$	98.0	-8.95	-5.21	-3.74	-5.01	-1.64	-3.37	-8.9	$16a_g$	93.4	-9.98	-6.44	-3.54	-10.8
$11a_g$	93.0	-9.18	-5.60	-3.58	-5.53	-2.06	-3.47	-9.4	$8b_g$	96.7	-10.35	-6.65	-3.70	-10.4
$5b_g$	69.1	-9.32	-6.24	-3.08	-5.61	-2.44	-3.17	-9.4	$15a_g$	92.4	-10.19	-6.88	-3.31	-11.4
$11b_u$		-9.20	-6.64	-2.56	-6.57	-4.04	-2.53	-10.2	$7b_g$	72.2	-10.38	-7.18	-3.20	-11.4
$10a_g$	4.2	-10.50	-7.98	-2.52	-7.94	-5.38	-2.56	-11.4	$14a_g$	40.2	-10.57	-7.39	-3.18	-12.0

[a] E_T', E_G', and Δ' are from Fenske's work.[3k] Data of %Ni 3d, E_T, E_G, and Δ are from this work. E_T'' is from ref 3t.

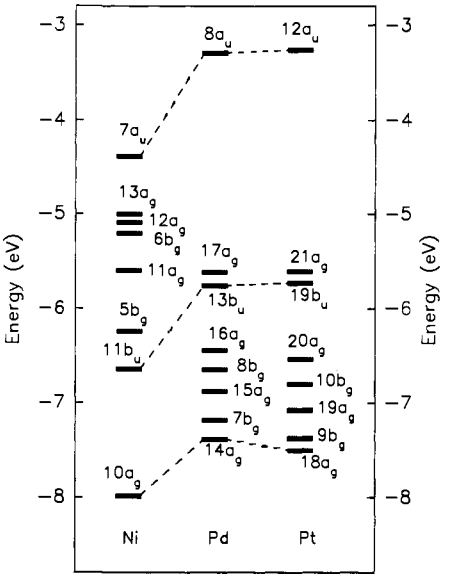

Figure 9. Our Xα–SW MO ordering for M(η^3-C_3H_5)$_2$ (M = Ni, Pd, and Pt).

$$\sigma_i \propto \sum_j (P_{A_j})_i \sigma_{A_j} \qquad (1)$$

where $(P_{A_j})_i$ is given approximately by the orbital composition from our Xα calculations and σ_{A_j} are the theoretical atomic cross sections as a function of photon energy. In this work, Yeh and Lindau's data[26] obtained by the Hartree–Slater central field method were used. Because most of the orbitals are largely atomic (e.g., metal d or C 2p) in nature, an excellent qualitative guide to the variations in molecular cross sections and branching ratios can be obtained directly by looking at the important atomic cross sections and ratios of cross sections of M nd/C 2p in Figure 10. Thus, all three metal d orbitals show a large increase in cross section above the threshold, before decreasing in markedly different ways at higher energies. In contrast, the C 2p orbitals show a monotonic decrease in cross section over the whole range. This behavior gives rise to the very large changes in the ratio of the M nd/C 2p cross sections, which are reflected in the branching ratio changes shown. This ratio (Figure 10b) increases drastically above the threshold for all three metals but decreases for Pd and Pt above ~50 eV. For Pd, there is a marked minimum in this ratio at ~110 eV, due to the Cooper minimum in the atomic Pd 4d cross section.

The Xα cross sections plotted in Figures 11–13 reflect the atomic cross sections in Figure 10a and provide a powerful way of assigning the photoelectron peaks. The five mainly metal MO's are clearly distinguished from the mainly ligand MO's, with the bonding MO's having intermediate behavior. This distinction is very clear for all energies for Ni(η^3-C_3H_5)$_2$ results (Figure 11) and the low-energy Pd(η^3-C_3H_5)$_2$ results (Figure 12a). However,

(26) Yeh, J. J.; Lindau, I. *At. Nucl. Data Tables* **1985**, *32*, 1.

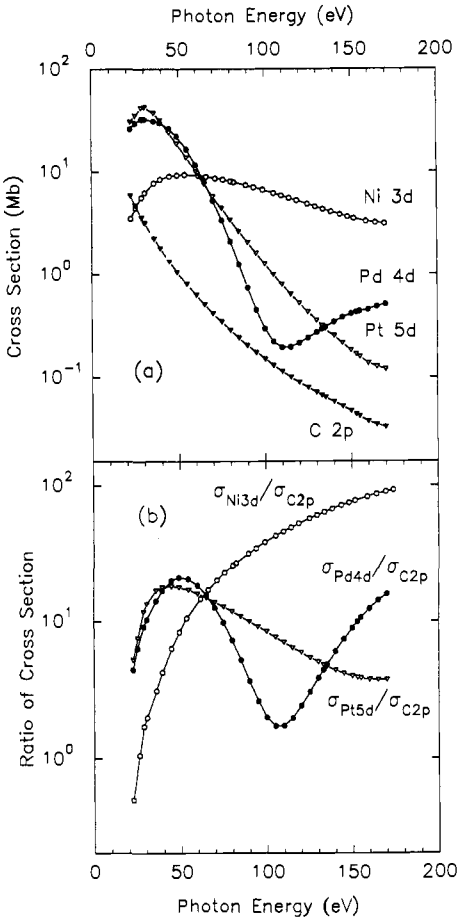

Figure 10. (a) Photoionization cross sections for atomic Ni 3d, Pd 4d, Pt 5d, and C 2p subshells.[26] (b) Ratio of atomic cross sections $\sigma_{M\ nd}/\sigma_{C\ 2p}$.

for the high-energy Pd results (Figure 12b), the mainly Pd 4d orbitals have their cross section fall below the ligand cross sections at the Pd 4d Cooper minimum. This "reversal" of Pd 4d and ligand cross sections shows how important it is to study the cross section behavior over a relatively wide energy range.

Discussion

The MO calculations (see Tables 1 and 2) all give eight MO's in this outer valence region. The Pt spectrum gives exactly eight photoelectron bands, whereas the Pd spectrum gives seven bands and the Ni spectrum only six bands. However, band 6 is clearly very broad in the Pd spectrum (Figure 1) and can be "resolved" into two peaks. Our high-resolution Ni spectrum (Figure 2) enables us to "resolve" the additional two peaks with some confidence in this spectrum. Thus, we can readily identify the expected eight peaks for all three molecules. However in the Ni case, we can only compare cross sections for the six band fits as shown in Figure 4. Clearly, there are many closely overlapping

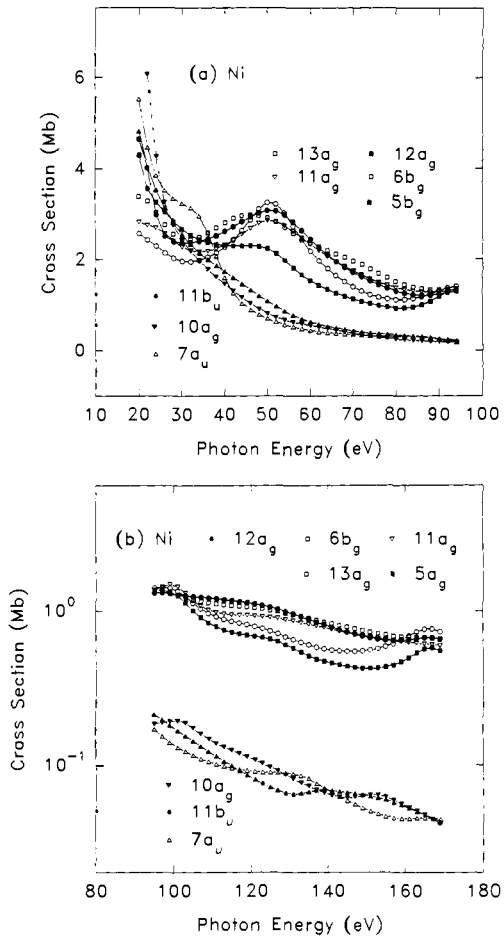

Figure 11. Xα–SW photoionization cross sections of $Ni(\eta^3\text{-}C_3H_5)_2$ (a) from 20 to 95 eV and (b) from 95 to 170 eV (on log scale).

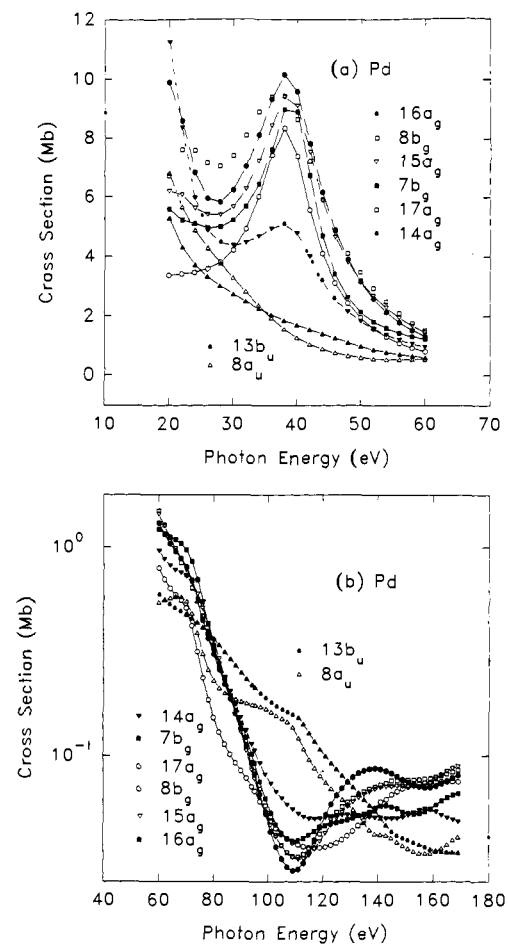

Figure 12. Xα–SW photoionization cross sections of $Pd(\eta^3\text{-}C_3H_5)_2$ (a) from 20 to 60 eV and (b) from 60 to 170 eV (on log scale).

peaks (especially for $Ni(\eta^3\text{-}C_3H_5)_2$), which makes any theoretical assignment based on energies incredibly difficult.[38] Our challenge is to match the observed and theoretical branching ratios. Our assignments based on this matching are given in Table 1.

(a) Assignment for $Ni(\eta^3\text{-}C_3H_5)_2$. Following Böhm's assignment and numerous theoretical studies, it has been generally agreed that the lowest ionization energy band (band 1 in Figure 4) in the photoelectron spectrum of $Ni(\eta^3\text{-}C_3H_5)_2$ was due to the ligand orbital $7a_u$. However, the spectra illustrated in Figures 4 and 7 show clearly that the relative intensity of the first ionization band increases with photon energy and so *must* be associated with an orbital having mostly nickel 3d character.[10] Actually, five bands are expected in the region where bands 1–3 (Figure 4) are observed and an expansion of the high-resolution He I and He II spectra shown in Figure 2 does indeed give some evidence for five bands, though they are not clearly resolved. Thus, bands 1A,B (Figure 2) combine to give band 1 (Figure 4) and bands 2A,B (Figure 2) give band 2 (Figure 4). The relative intensity of band 2B decreases markedly from He I to He II spectra (Figure 2) and so it is assigned to the ligand $7a_u$ orbital, with the other bands due to orbitals with mostly nickel 3d character. The intensity of band 4 does not decrease nearly as much as those of bands 5 and 6 with increasing photon energy (Figures 4 and 7), and so band 4 is assigned to the bonding orbital $5b_g$ (having both Ni 3d and ligand C 2p characters) while bands 5 and 6 are assigned to ligand orbitals.

Our assignment is confirmed by the good agreement between both Gelius and Xα–SW branching ratios with the experimental ratios between 21 and 80 eV (Figure 14). Thus, the BR for band 1 is large and increases markedly. This band *must* be assigned to *two* orbitals of very *high Ni 3d* character (Table 1). The BR for band 2 is large but relatively flat: this band must be assigned to a Ni 3d orbital *plus* the ligand $7a_u$ orbital. The BR for band 3 is much smaller ($\sim$10%) and increases slightly: it is assigned to one metal orbital ($11a_g$) of lowest Ni 3d character. The BR for band 4 is rather small ($\sim$10%) and decreases slightly: it is assigned to the bonding $5b_g$ orbital. Finally, bands 5 and 6 have branching ratios which decrease dramatically: they are assigned to the ligand orbitals $11b_u$ and $10a_g$, respectively. The intensity changes at higher energy (Figure 7) are consistent with this assignment. We feel that this assignment is now on a firm footing. However, of course, we cannot distinguish the ordering of the four metal 3d orbitals ($13a_g$, $12a_g$, $6b_g$, and $11a_g$) readily using our intensity arguments, although all calculations put the $13a_g$ orbital as the lowest binding energy 3d orbital. It is possible then that the $12a_g$, $6b_g$, and $11a_g$ orbital assignments could be interchanged, but we rely on the energy ordering obtained from our Xα calculations on the Ni complex and the same theoretical ordering obtained by us for the Pd and Pt complexes.

It must be noted that our assignment is very different from that obtained in any previous studies including our own preliminary study without MS–Xα calculations.[10] Of greatest note, the first peak is due to *two* Ni 3d orbitals and not the *one* ligand $7a_u$ orbital.[3] This assignment is not in agreement with either the Xα–SW ground state orbital energies *or* the transition state energies, which should better approximate the IP's. The $7a_u$ orbital must be associated with peak 2 (peak 2B in Figure 2).

Apart from this discrepancy, our assignment is consistent with the rest of our MS–Xα energy ordering and most of the ordering given in the latest Xα–SW calculations.[3t] However, even the remaining assignment is *very* different from that given in previous papers (see, for example, Table V in ref 3k and Table 6 in ref 3g). For both the above assignments, only their assignment of $11b_u$ to band 5 agrees with our assignment; every other band is

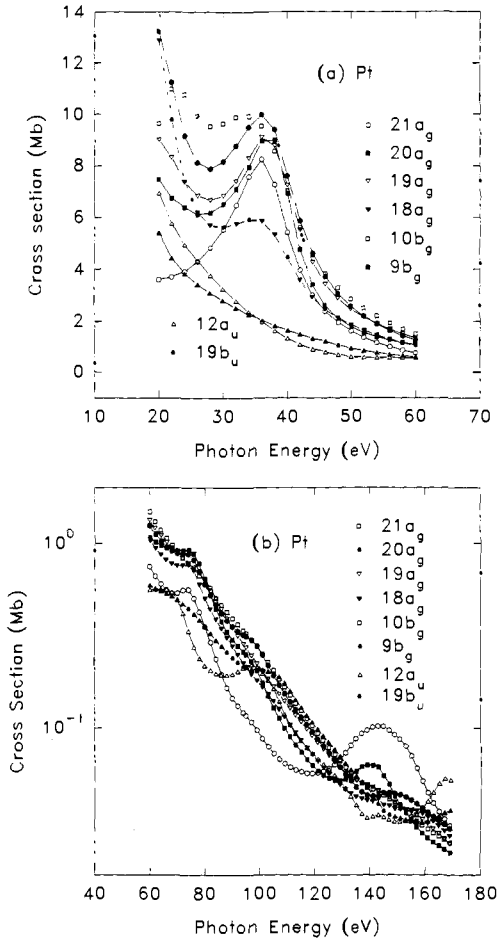

Figure 13. Xα–SW photoionization cross sections of Pt(η^3-C_3H_5)$_2$ (a) from 20 to 60 eV and (b) from 60 to 170 eV (on log scale).

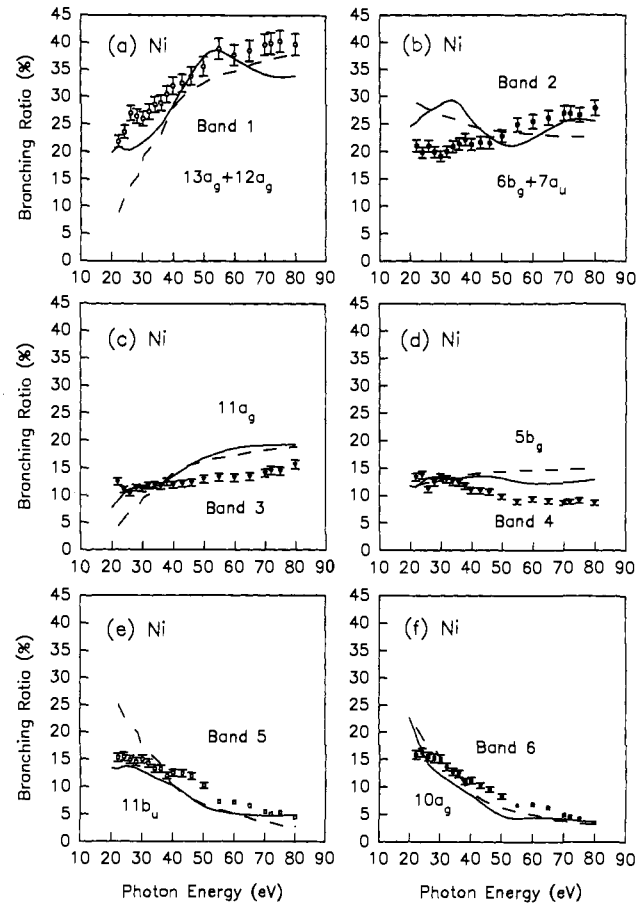

Figure 14. Comparison of experimental branching ratios (circle, triangles, and squares) with Xα ones (solid lines) and ones from the Gelius model (dashed lines) for the six valence bands of Ni(η^3-C_3H_5)$_2$ in the photon energy range 20 to 80 eV. Our band assignments are indicated on each plot.

assigned differently! Also, our present assignment differs from that given by us[10] because we used the orbital characters from the INDO calculation,[3g] which are quite different from those from the Xα calculation.[27]

(b) Assignments for Pd(η^3-C_3H_5)$_2$ and Pt(η^3-C_3H_5)$_2$. The lowest energy band in the photoelectron spectra of Pd(η^3-C_3H_5)$_2$ decreases in intensity as the photon energy increases from He I to 90 eV (Figure 5) and hence is assigned to the ligand 8a_u orbital. The next four bands (bands 2–5) are then assigned to the orbitals with mostly nonbonding palladium 4d character, since these intensities all increase with increasing photon energies over this energy region (Figure 5). Note that band 2 is assigned to the 17a_g orbital, which has the lowest Pd 4d character of these four orbitals. Figure 5 shows clearly that the intensity of band 2 decreases relative to bands 3, 4, and 5 as expected from this assignment. Finally, band 6 is assigned to the combination of the metal–ligand bonding orbital 7b_g and the ligand orbital 13b_u, while band 7 is assigned to the ligand orbital 14a_g. Apart from the change in relative position of the ligand a_u orbital between Ni and Pd, the remaining ordering for the two molecules is the same. Note that this assignment (Tables 1 and 2) means that the 13b_u orbital position from MS–Xα energies is in poor agreement with experiment.

At higher photon energies, the relative intensities of Pd 4d bands 2–5 decrease to a minimum at about 120 eV and then increase again (Figure 8). This is due to the expected Pd 4d Cooper minimum (Figure 10),[9] and the observation of this effect lends strong support to the assignment. This is the first time that the 4d Cooper minimum has been observed for a gas phase palladium complex. The observed and calculated branching ratios in Figure 15 confirm this assignment. The positions of the maximum and minimum are shifted to high energy compared to the theoretical values, but the overall qualitative agreement is remarkably good between the experimental results and both theoretical calculations.

The high-resolution spectrum of the first two bands for the Pd complex (Figure 3) are consistent with the above assignment. As mentioned previously the vibrational frequencies derived from Figure 3 are in the range 1130∼1300 cm^{-1}, close to the ground state vibrational frequencies, 1009∼1029 cm^{-1} of C–C–C stretching modes for solid state Pd(η^3-C_3H_5)$_2$. More vibrational structure on the ligand MO (8a_u) than on the metal-based MO (17a_g) is certainly expected.

The assignments for Pt(η^3-C_3H_5)$_2$ are very similar to those for Pd(η^3-C_3H_5)$_2$. Again the intensity of the lowest energy band falls with increasing energy over the range 21.1–90 eV (Figures 1 and 6) and is assigned to the ligand 12a_u orbital (Table 1). The next four bands (2–5) are assigned to the orbitals with mostly platinum 5d character since the intensities increase from 21.2 to 90 eV. Band 6 is assigned to the bonding orbital 9b_g and bands 7 and 8 to the ligand orbitals 19b_u and 18a_g, respectively. It can be seen from Tables 1 and 2 that the sequence is different from that calculated by the Xα method for the ground state and transition state, but the assignments for the palladium and platinum complexes are less controversial than for nickel and are in agreement with the assignments made by Böhm.[3g,h] The extra

(27) In ref 10, the 13a_g orbital from ref 3g had only 66.6% Ni 3d character and the theoretical and experimental branching ratios better matched if 13a_g was assigned to peak 3. Obviously, the assignment is somewhat dependent on the orbital characters. However, the good agreement for both Ni and Pd branching ratios with both the Gelius and Xα theoretical values strongly indicates that the Xα orbital characters are closer to being correct than either the ab initio or INDO characters: there is very little orbital mixing between metal and ligand orbitals.

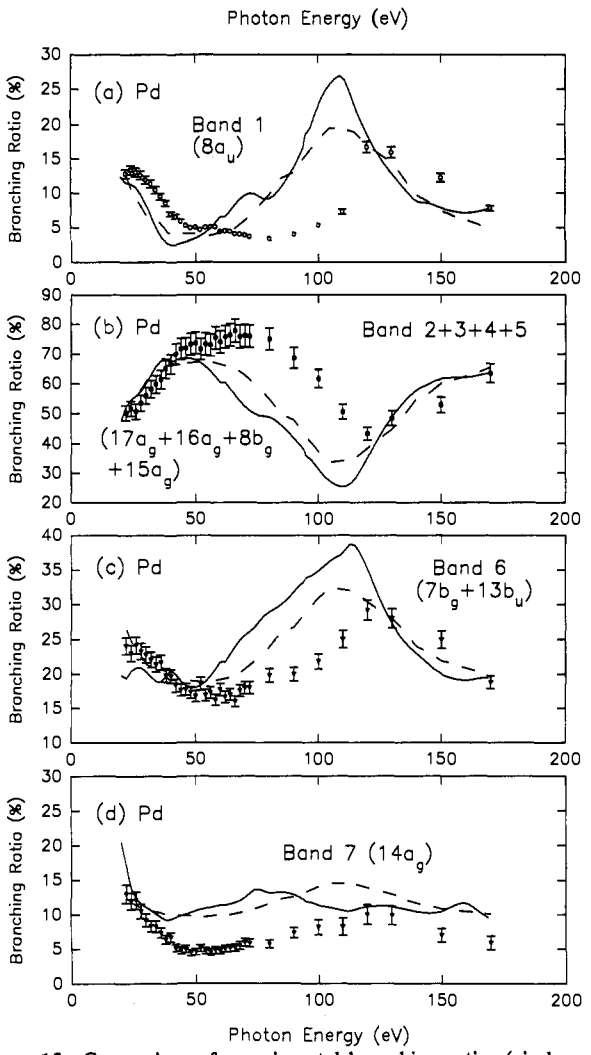

Figure 15. Comparison of experimental branching ratios (circles and triangles) with Xα ones (solid lines) and the ones from the Gelius model (dashed lines) for the seven valence bands of $Pd(\eta^3\text{-}C_3H_5)_2$ in the photon energy range 20 to 170 eV. Band assignment are indicated on each plot.

intensity data obtained from this synchrotron study put the assignments for the Pd and Pt complexes on a very firm basis.

(c) Transition State Calculations: The Effects of Charge and Relaxation. Although we feel that the assignment of these spectra is now firm, we have to discuss whether the ground state MO ordering is the same as that given from the spectra. Or in other words, is Koopmans' theorem valid for these molecules?

The Xα transition state calculation makes allowance for charge effects and for relaxation effects which, based on previous studies, are expected to influence the observed binding energies and often give a good approximation to the experimental ionization energies.[3k] The calculated transition state eigenvalues should therefore contain allowance for the following effects:[3k]

(1) MO's with mostly metal d character should be affected mostly by the charge effect, since they approximate most closely localized atomic orbitals. Delocalized ligand MO's should be stabilized to a considerably lower extent because the charge is delocalized over several atoms.

(2) Reorganization effects are expected to be greater for metal than for ligand MO's, and this should therefore counterbalance the charge effect to a greater or lesser extent. The theory is that removal of charge from a metal MO leads to considerable charge migration toward the metal, thus leading to a *lower* ionization energy than expected according to Koopmans' theorem.

(3) Reorganization effects are often thought to be greatest for the first transition series elements, following the sequence 3d > 4d or 5d.[4,5]

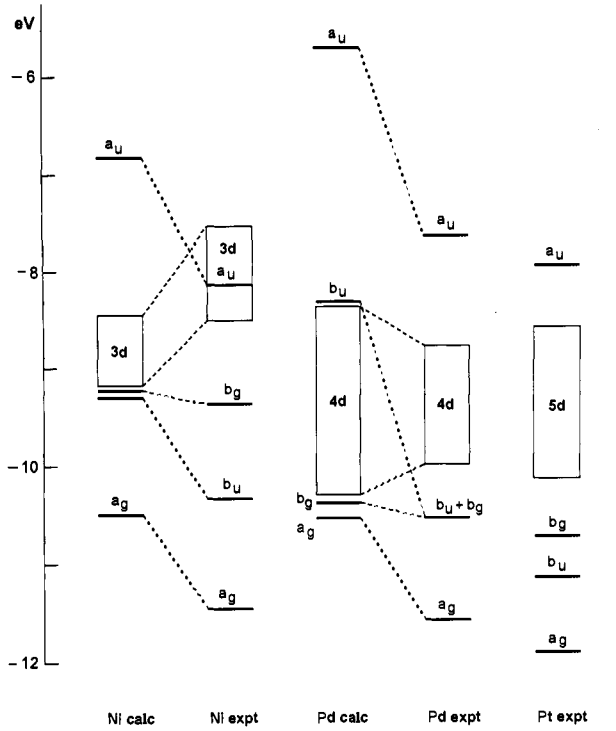

Figure 16. Schematic MO diagrams for $M(\eta^3\text{-}C_3H_5)_2$ from Xα calculations (the Pt calculation is omitted because it is very similar to the Pd calculation) and the experimental binding energy ordering from the assignment based on variable photon energy photoelectron spectroscopy.

The following trends in Δ (=$E_T - E_G$), where E_T and E_G are the transition state and ground state Xα eigenvalues, respectively, are found (Table 2). For $Ni(\eta^3\text{-}C_3H_5)_2$, there is good agreement between the present work and the work of Fenske[3k] and Guerra.[3t] The orbitals with mostly metal d character are stabilized to the greatest extent in the transition state. Thus Δ ≈ −3.5 eV for orbitals with mostly metal d character, while Δ ≈ −2.5 eV for orbitals with mostly ligand character. Hence the calculation predicts that the charge effect dominates over the relaxation effect in the transition state. Secondly, the Δ values are very similar for both $Ni(\eta^3\text{-}C_3H_5)_2$ and $Pd(\eta^3\text{-}C_3H_5)_2$. Hence the balance between charge effects and relaxation effects appears to be about the same in both cases. For example, the *magnitudes* of both the reorganization energies and the charge effect must be in the order 3d > 4d, but the very similar values are not consistent with differences in reorganization energy between Ni and Pd of a few electronvolts as has been suggested.[4,5] Indeed, it seems to us that the Ni 3d orbital(s) could still be the HOMO in the ground state (see the next section). Obviously more theoretical work is required!

Equally obvious is that the Xα transition energies do not give the correct sequence of IP's. The comparison of the Xα calculated transition state energies with the observed binding energies is shown in Figure 16. It can be seen that, for both the nickel *and* palladium complexes, the observed binding energies are greater than the calculated values for the orbitals with mostly ligand character, less than the calculated values for the orbitals with >90% metal d character, and less than the calculated values for the b_g orbitals with both metal and ligand character (b_g). This could be rationalized if the calculation underestimates the degree of covalency in the complexes. The charge on nickel has been calculated by the Xα method to be +0.3e with corresponding charge of −0.15e on each η^3-allyl group. A nonpolar molecule would have lower binding energies for metal orbitals and higher binding energies for ligand orbitals.

(d) Trends in Metal d Orbital Energies for $M(\eta^3\text{-}C_3H_5)_2$. The most significant trend for the compounds $M(\eta^3\text{-}C_3H_5)_2$ (M = Ni,

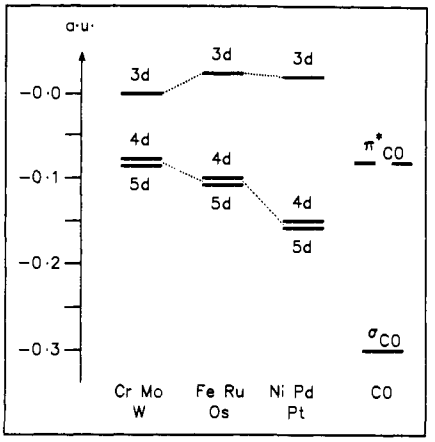

Figure 17. Average d orbital energies relative to CO valence MO's for Cr, Fe, and Ni triads from Ziegler's summary.[30]

Pd, Pt) is in the average IP's for the 10 d electrons. The IP's follow the series M = Ni (8.26 eV) < M = Pd (9.64 eV) ≈ M = Pt (9.62 eV). The difference between the values for M = Ni and M = Pd or Pt of >1 eV is large. For comparison, the reported ionization potentials[28] of d based MO's (t_{2g}) in $M(CO)_6$ (M = Cr, Mo, and W) are $Cr(CO)_6$ (8.40 eV) < $Mo(CO)_6$ (8.50 eV) < $W(CO)_6$ (8.56 eV), showing only a 0.1 eV difference between the first and second rows, and for $M(\eta^5\text{-}CH_3C_5H_4)_2$ (M = Fe, Ru, and Os), the corresponding values are $Fe(\eta^5\text{-}CH_3C_5H_4)_2$ (6.89 eV) < $Ru(\eta^5\text{-}CH_3C_5H_4)_2$ (7.25 eV) ≈ $Os(\eta^5\text{-}CH_3C_5H_4)_2$ (7.23 eV), which yield a difference of 0.36 eV between the first and second rows. A large separation between the metal d IP's for first and second row organometallics has also been found in $CpM(CO)_2$ (M = Co and Rh)[4] and other cobalt group organometallic compounds.[29]

What is the reason for this trend, in which the energy difference between 3d and 4d or 5d orbitals for equivalent compounds appears to increase for the later transition metals? Lichtenberger *et al.* attributed the d IP separation in $CpM(CO)_2$ (M = Co and Rh) mainly to the bigger relaxation energy associated with first row d^8 and d^{10} complexes, which was considered to be about twice that of second row metal ionizations.[4,5] On the other hand, Ziegler *et al.*[30] proposed that trends in the thermal stability and kinetic lability of the metal–carbonyl bond in $M(CO)_6$ (M = Cr, Mo, and W), $M(CO)_5$ (M = Fe, Ru, and Os), and $M(CO)_4$ (M = Ni, Pd, and Pt)[30] were due to the ground state energy differences between the first and second or third row transition metals. They suggested that, in the ground state, the 4d and 5d metal orbitals are lower in energy than the 3d since d–d repulsions are smaller for the diffuse 4d and 5d orbitals than for the contracted 3d orbitals and that this difference should increase from left to right in the transition metal row of the periodic table. Due to the "lanthanide contraction", the energies of 4d and 5d metal orbitals are relatively close. The average orbital energy levels of metals with d^6, d^8, and d^{10} configurations relative to the HOMO and LUMO of CO were calculated as in Figure 17;[30] the d separation is larger for the nickel group than for the Cr and Fe groups. The Xα calculations carried out for $Ni(\eta^3\text{-}C_3H_5)_2$ and $Pd(\eta^3\text{-}C_3H_5)_2$ in the present work support Ziegler's interpretation in terms of the difference in ground state d orbital energies. We note that, for organometallic compounds of the nickel group, back-bonding from filled d orbitals to π* orbitals of the ligands usually follows the sequence Ni ≫ Pd < Pt, which suggests higher energy d orbitals for M = Ni. For example, the existence of $Ni(CO)_4$ but not $Pd(CO)_4$ or $Pt(CO)_4$ as stable complexes is usually interpreted in terms of a better energy match between metal d orbitals and π*(CO) orbitals for M = Ni. The very different reactions of olefins on Ni versus Pt surfaces[31,32] may also be largely due to the enhanced π bonding on Ni surfaces.

Table 3. Xα MO Ordering and Compositions for *cis*-$M(\eta^3\text{-}C_3H_5)_2$

Ni orbital	energy (eV)	Ni %s	Ni %p	Ni %d	middle C %p	terminal C %p
$8b_1$	−3.81		9.9	36.9		50.6
$10b_2$	−4.12			78.8	3.2	12.7
$14a_1$	−4.91			96.5		
$7b_1$	−5.40			76.4	1.3	20.3
$13a_1$	−5.43			93.5	3.6	1.9
$5a_2$	−6.02			70.4	2.2	25.1
$9b_2$	−6.95		3.0	22.7	37.2	30.3
$12a_1$	−8.08	15.7			34.7	40.7
Pd orbital	**energy (eV)**	**Pd %s**	**Pd %p**	**Pd %d**	**middle C %p**	**terminal C %p**
$10b_1$	−3.18		10.5	5.4		80.5
$12b_2$	−4.44		5.2	49.7	17.0	26.8
$18a_1$	−6.08	3.7		89.4	2.1	2.9
$9b_1$	−6.55			92.9	2.0	4.7
$17a_1$	−6.69			87.7	8.8	1.5
$6a_2$	−7.07			75.2	4.3	18.5
$16a_1$	−7.08	7.6		28.3	25.4	34.9
$11b_2$	−7.10			52.5	22.9	17.9
Pt orbital	**energy (eV)**	**Pt %s**	**Pt %p**	**Pt %d**	**middle C %p**	**terminal C %p**
$14b_1$	−3.13		13.0	5.1		78.0
$16b_2$	−4.32		7.1	47.6	16.1	27.6
$24a_1$	−6.11	6.2		84.9	2.8	3.8
$13b_1$	−6.70			91.7	2.5	5.3
$23a_1$	−6.86			78.9	13.6	3.8
$8a_2$	−7.28			71.3	5.6	20.6
$22a_1$	−7.18	6.8		42.1	18.2	29.4
$15b_2$	−7.24			50.3	23.2	18.6

According to the Xα calculations, the highest energy ligand-based orbitals are $7a_u$, $8a_u$, and $12a_u$ for $Ni(\eta^3\text{-}C_3H_5)_2$, $Pd(\eta^3\text{-}C_3H_5)_2$, and $Pt(\eta^3\text{-}C_3H_5)_2$, respectively. The energies are similar and the IP sequence is as follows: $7a_u$ (Ni, 8.15 eV) > $12a_u$ (Pt, 7.91 eV) > $8a_u$ (Pd, 7.64 eV). This is consistent with the view that bonding overlap with the empty metal p orbital will stabilize the a_u orbital.

(e) Electronic Structures of *cis* Isomers of $M(\eta^3\text{-}C_3H_5)_2$. The photoelectron and theoretical studies have normally assumed that the *trans* compounds are present in the gas phase. Batich[3c] believed that the presence of two isomers should just broaden the PES peaks, and all later studies have only considered the *trans* species. However, ^{13}C NMR data at below room temperature have shown that in toluene-d_8 solution about 70% of the compound is *trans* while about 30% is *cis*.[13] Our NMR results confirm these solution results. There still has to be some doubt, then, as to the isomeric composition of these complexes in the gas phase.

To further examine this problem we performed Xα–SW calculations for the *cis* isomers. The calculated MO energies compositions are listed in Table 3. More than 20 years ago, Hillier and Canadine did the MO calculation for *trans*- and *cis*-$Pd(\eta^3\text{-}C_3H_5)_2$ using the self-consistent charge with electron interaction method.[6] Their results show similar eigenvalues, atomic charges and configurations, and overlap populations for the two isomers.

As for the *trans* isomer, the four π ligand orbitals in *cis*-$M(\eta^3\text{-}C_3H_5)_2$ are in-phase and out-of-phase combinations of the molecular orbitals of the individual allyl radical groups. Their electron configurations are $(core)(a_1)^2(b_2)^2(b_1)^2(a_2)^0$. *cis*- and *trans*-$M(\eta^3\text{-}C_3H_5)_2$ have C_{2v} and C_{2h} symmetries, respectively. The different symmetries do affect the metal–allyl bonding. For

(28) Cowley, A. H. *Prog. Inorg. Chem.* **1979**, *26*, 46.
(29) (a) Green, J. C.; Powell, P.; van Tilborg, J. E. *Organometallics* **1984**, *3*, 211. (b) Dudeney, N.; Kirchner, O. N.; Green, J. C.; Maitlis, P. M. *J. Chem. Soc., Dalton Trans.* **1984**, 1877.
(30) Ziegler, T.; Tschinke, V.; Ursenbach, C. *J. Am. Chem. Soc.* **1987**, *109*, 4825.
(31) Hammer, L.; Müller, K. *Prog. Surf. Sci.* **1991**, *35*, 103.
(32) Avery, N. R.; Sheppard, N. *Proc. R. Soc. London, A* **1986**, *405*, 1, 27.

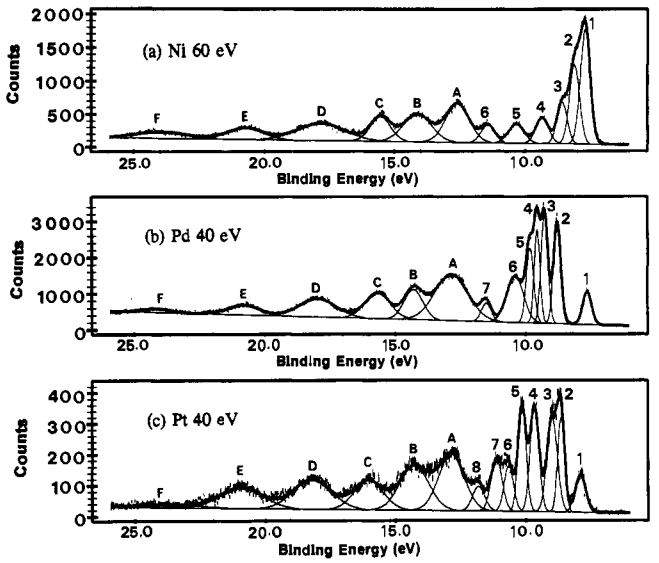

Figure 18. Broad range PE spectra of M(η^3-C_3H_5)$_2$ (M = Ni, Pd and Pt) at 60, 40, and 40 eV, respectively, showing the similarity of the inner valence shells among these three compounds.

example, in the C_{2h} *trans* structure, the two ligand orbitals a_u (π) and b_u(π) are forbidden by symmetry to mix with the metal d orbitals which all have g symmetry, and so several orbitals have pure ligand or metal character. In the C_{2v} structure, all four ligand π MO's can interact with a metal d orbital. So, with matching symmetry, mixing of ligand and metal orbitals occurs to a much greater extent in the *cis* isomer.

The MO eigenvalues and compositions of *cis*-M(η^3-C_3H_5)$_2$ are listed in Table 3. Our MO ordering of *cis*-Pd(η^3-C_3H_5)$_2$ is not in particular good agreement with that reported by Hillier and Canadine. Their HOMO and the lowest MO in the outer valence region are different from ours.

Comparing the energies and orbital characters for the *trans* and *cis* isomers (Tables 1 and 3, respectively), there are strong similarities. Thus, apart from the first two b_1 and b_2 MO's, the MO energies for the next six MO's all agree to within 0.3 eV. As for the *trans* compounds, the five mainly d MO's in the *cis* compounds are sandwiched between the three mainly ligand MO's. As expected from the qualitative arguments above, there is much more mixing of the d and ligand MO's in the *cis* molecules and one or both of the first two low-energy MO's in the *cis* compounds should have a noticeably lower binding energy than in the *trans* compound. These latter two observations suggest that there is no observable *cis* compound (<20% of *trans*) in our spectra. For example, in the Pd and Pt complexes, the theoretical results suggest that there should be *two* peaks (from b_1 and b_2) between 7.6 and 8.8 eV of binding energy. The spectra (Figure 1) shows no hint of two resolvable peaks. Perhaps more convincingly, the calculation on *cis*-Ni(η^3-C_3H_5)$_2$ shows that the $9b_2$ orbital (which would be assigned to peak 5) has substantial d character. The very strong and parallel decrease of B.R. for both peaks 5 and 6 (Figure 14e,f) suggests strongly that *both* these peaks correspond to orbitals with little or no metal d character (as seen for the *trans* isomer in Table 1).

(f) Inner Valence Spectra. The broad-range high-resolution photoelectron spectra of the three complexes are shown in Figures 18 and 19. These complete valence and inner valence spectra, and those of other organometallics,[33] are the first high-resolution spectra to be published for organometallic molecules. All the valence peaks are readily seen in these spectra at high resolution. In addition, the broad inner valence peaks[34] are also evident.

(33) Hu, Y. F.; Bancroft, G. M.; Tan, K. H. *J. Am. Chem. Soc.*, submitted for publication.

(34) The designation of inner valence here is arbitrary. In fact, peaks A, B, and C of mainly C 2p and H 1s character would normally be considered as valence ionizations.

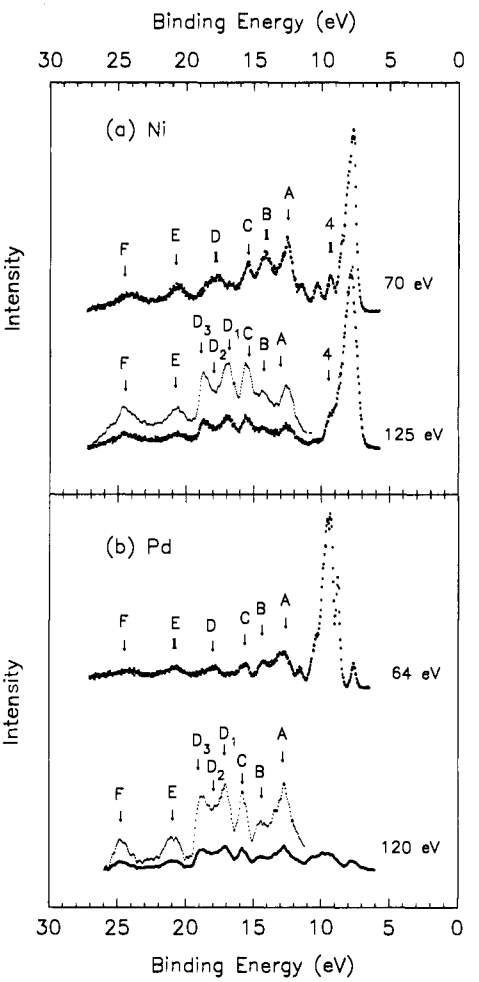

Figure 19. Comparison of PE spectra of Ni(η^3-C_3H_5)$_2$ (at 70 and 125 eV) and Pd(η^3-C_3H_5)$_2$ (at 64 and 120 eV).

Table 4. Xα MO Energy and Mainly Composition[a] of Ni(η^3-C_3H_5)$_2$

region[b]	orbital	energy (eV)	assignment	IP (eV)	%C 2p	%C 2s	%H 1s
	$10b_u$	−9.77			49.9		47.8
	$6a_u$	−9.89	A	12.6	59.6		39.4
	$9a_g$	−9.92			48.3		44.5
(p)	$4b_g$	−9.97			57.8		37.6
	$5a_u$	−11.42	B	14.2	70.9		28.6
	$3b_g$	−11.52			68.1		30.3
	$9b_u$	−12.48	C	15.6	59.0	2.6	36.9
	$8a_g$	−12.70			58.1		36.3
(p–s)	$8b_u$	−14.59	D	17.9	23.7	33.8	42.0
	$7a_g$	−14.67			23.1	34.6	41.1
	$2a_g$	−17.37	E	20.8	14.2	59.9	23.2
(s)	$4a_u$	−17.41			13.8	60.4	24.0
	$7b_u$	−20.50	F	24.0	8.0	78.4	10.6
	$6a_g$	−20.78			6.4	76.8	9.9

[a] %Ni is less than 4.44 for all orbitals. [b] Region is divided according to C 2p and C 2s composition. IP errors < ±0.05 eV.

These high-quality spectra, taken in less than 10 min, demonstrate the power of our photoelectron spectrometer combined with monochromatized synchrotron radiation.

The theoretical MO energies and orbital compositions for Ni(η^3-C_3H_5)$_2$ from our ground state Xα–SW calculations are listed in Table 4, along with our experimental photoelectron energies and our assignments. (The inner valence energies for the Pd complex agree with those of the Ni complex to within 0.1 eV.) We can divide the inner valence region into three regions based on the C 2p and C 2s compositions of the MO's (there is little or no Ni component to these MO's as expected). The first region (from $10b_u$ at −9.77 eV to $8a_g$ at −12.70 eV) contains eight MO's of high C 2p character. These eight MO's divide naturally into

three subregions. The MO's in each subregion have very similar energies, leading naturally to the assignments of peaks A, B, and C in Table 4. The second s–p region contains only two MO's of mixed C 2p and C 2s character, and these two MO's are associated with peak D. Finally, the third region contains four MO's of mainly C 2s character, and these two pairs of MO's are associated with peaks E and F. Note that the experimental IP's are all about 3 eV larger than the ground state theoretical values (as also seen in Table 1 for the valence orbitals). This good agreement between experiment and theory suggests that our assignment is on a firm footing.

Spectra at higher photon energies (Figure 19) show two features which are expected. First, the 120 eV spectra for both Ni and Pd complexes are very similar. Second, peaks A, B, and C at 120 eV for both compounds become much weaker (relative to peaks D, E, and F) compared to the lower energy spectra. This is expected from the trends in C 2p and C 2s cross sections[26] which show the C 2p cross section decreasing more rapidly than the C 2s cross section at higher photon energies. However, there are two very unexpected features in the 120 eV spectra. First, and most surprising, peak D splits into at least two peaks D_1 and D_3, on either side of peak D (=D_2). Second, the intensities of E and F do not increase substantially as expected due to the high C 2s character of the orbitals associated with these peaks. Because the Pd and Ni spectra both show these effects, neither of these effects can be due to effects such as ionization of metal core orbitals by second-order radiation or multielectron resonance effects from core level excitation/ionization.[35]

The latter two effects cannot be explained fully without further experimental and theoretical work. However, a brief discussion here outlines the most likely qualitative explanation. In the outer valence region, there is usually a one to one correspondence between the photoelectron peaks and molecular orbitals. However, in the inner valence region, electron–electron correlation often gives rise to additional peaks.[10,36-39] Good examples of these effects in small molecules have been seen recently in CO[16] and C_2H_4.[38,39] Indeed, the intensity of a new correlation satellite in $C_2H_4$39 shows a strong intensity fluctuation with photon energies between 30 and 90 eV. This satellite is considered to be due to "dynamic" correlation rather than the usual "intrinsic" correlation. It would appear that the strong intensity fluctuations in peak D are due to such dynamic correlation, although the extremely large change above 100 eV is not expected from previous results.

(35) Cooper, G.; Green, J. C.; Payne, M. P.; Dobson, J.; Hullier, I. H. *J. Am. Chem. Soc.* **1987**, *109*, 3836. Brennan, J. G.; Cooper, G.; Green, J. C.; Kaltsoyannis, N.; MacDonald, M. A.; Payne, M. P.; Redfern, C. M.; Sze, K. H. *Chem. Phys.* **1992**, *164*, 271 and references therein.

(36) Cederbaum, L. S.; Domcke, W.; Schirmer, J.; von Niessen, W. *Adv. Chem. Phys.* **1986**, *65*, 115.

Conclusions

There has been a long-standing controversy over the assignment of both the photoelectron spectra and the ground state MO ordering in the three complexes $M(\eta^3\text{-}C_3H_5)_2$. Our detailed variable energy photoelectron study combined with theoretical energy and intensity analysis now puts the assignment of the photoelectron spectra on a much more firm footing. The relative intensities for the different ligand and metal valence photoionizations show very different energy trends which are predicted theoretically. This agreement enables us to assign the photoelectron spectra with confidence. The MS–Xα energies generally are in good relative agreement with the theoretical analysis for both inner and outer valence regions with the exception of the $7a_u$ orbital in the Ni complex and the b_u orbital in the Pd and Pt complexes.

Our transition state MS–Xα calculation combined with other recent theoretical analyses indicates that the ground state MO ordering may not be very different from the ion state ordering. In particular, the relaxation energies for the Ni 3d orbitals do not appear to be more than 1 eV larger than for the Pd 4d or Pt 5d orbitals.

Acknowledgment. We are very grateful for the financial support of NSERC (Canada), for the continued assistance from the staff at the Aladdin Synchrotron, and for the other assistance from J. Z. Xiong, J. S. Tse, J. N. Cutler, D. G. J. Sutherland, and Z. F. Yin. We also acknowledge the support of NSR Grant No. DMR-9212658 to the Synchrotron Radiation Center.

(37) Becker, V.; Shirley, D. A. *Phys. Scr.* **1990**, *T31*, 56.

(38) Desjardins, S. J.; Bawagan, A. D. O.; Tan, K. H. *Chem. Phys. Lett.* **1992**, *196*, 261 and references therein.

(39) Desjardins, S. J.; Bawagan, A. D. O.; Tan, K. H. *Chem. Phys. Lett.* **1994**, in press.